High-pressure phases of liquid silane studied using first-principles molecular dynamics simulations

Y. H. Badjo,[1,2] B. Boates,[2,3] B. C. Saha,[1] and S. A. Bonev[2,*]

[1]*Department of Physics, Florida A&M University, Tallahassee, Florida 32307, USA*

[2]*Physical and Life Sciences Directorate, Physics Division, Lawrence Livermore National Laboratory, Livermore, California 94550, USA*

[3]*Machine Learning and Data Science, Cash App Block, San Francisco, California 94110, USA*

(Received 15 March 2024; revised 14 June 2024; accepted 14 June 2024; published 12 July 2024)

The structural and electronic transformations of liquid silane as a function of pressure are studied using first-principles molecular dynamics simulations. We present results for two isotherms, 1000 K and 2000 K, in the pressure range from ambient up to 265 GPa. The phases of dense liquid silane bear some similarities with its crystalline phases but there are significant differences as well. Notably, we find the emergence of a mixed polymeric-molecular H_2 phase with strong temperature dependence and metallization in the liquid occurring at significantly lower pressure than in the solid. We report dc conductivity, which reaches higher values, and has a different pressure dependence and physical origin than recent analysis of experimental measurements has suggested.

DOI: 10.1103/PhysRevB.110.024106

I. INTRODUCTION

The high-pressure behavior of hydrogen-rich compounds has attracted much attention following the proposition of Ashcroft [1] that they might exhibit exotic quantum properties, like high-temperature superconductivity, similar to what has been predicted for metallic hydrogen [2,3]. The hydrogen subsystem in these materials can be viewed as chemically precompressed, with the electron charge on the hydrogen atoms enhanced in comparison to that in the pure hydrogen system at the same pressure. Metallization in the hydrogen-rich compounds can therefore be expected at lower pressure than in pure hydrogen.

The hydrates of the group IV elements (C, Si, Ge), in particular, have attracted a lot of attention, leading to various fascinating discoveries for high-temperature superconductivity [4–11]. Among these, SiH_4 has been studied the most, with the majority of works focusing on its crystalline phases stable up to 300 GPa pressure and below room temperature [7,12,13]. At pressure between 10 and 25 GPa, solid SiH_4 forms a molecular monoclinic crystal [8,14] (with SiH_4 tetrahedra intact) with space group symmetry $P2_1/c$. Theoretical enthalpy calculations [8,9,15] predicted the emergence of solid structures consisting of SiH_6 octahedra (with $Fdd2$ symmetry) above 25 GPa and SiH_8 dodecahedra (space group $I4_1/a$) between 55 and 220 GPa. In these structures, every Si atom shares two H atoms with other Si atoms [8,10,16]. Upon further compression, a layered structure (*Pbcn* symmetry) consisting of nearly square Si layers separated by H interlayers was predicted [9] between 220–250 GPa, while subsequent structure searches [15] found the emergence of a metallic structure (space group $P-3$) above 250 GPa, characterized with the presence of H_2 pairs within the Si-H polymeric framework. Experimental measurements [17] at room temperature found the $I41/a$ structure to be stable up to 130 GPa.

Despite the interest in dense SiH_4, its properties at elevated temperatures and in the liquid phase are little known. Wang *et al.* [18] performed measurements on liquid silane from 1200 to 4100 K, where they determined it to remain molecular up to 90 GPa and dissociate above 100 GPa. The parallel between hydrogen-rich compounds and pure hydrogen suggests that SiH_4 may metallize at significantly lower pressure compared to solid SiH_4, and that thermal effects could lead to a rich finite-temperature phase diagram.

In this paper, we use first-principles molecular dynamics simulations to predict the phase diagram of liquid SiH_4 under high pressure up to 265 GPa, at 1000 K and 2000 K isotherms. The structural, dynamical, and electronic properties are obtained and discussed below.

II. COMPUTATIONAL METHODS

To study the phase transformations in liquid SiH_4 as a function of density and temperature, we have performed first-principles molecular dynamics (FPMD) simulations for two isotherms, namely, at 1000 and 2000 K in the density range corresponding to $1.40 \geqslant r_s \geqslant 2.10$, where $\frac{4}{3}\pi(r_s a_0)^3 = V/N$, a_0 being the Bohr radius, V the volume, and N the number of valence electrons. The calculations were carried out with the VIENNA AB INITIO SIMULATION PACKAGE (VASP) [19], using density functional theory (DFT) within the Perdew-Burke-Ernzerhof exchange correlation functional [20], Born-Oppenheimer dynamics, and finite-temperature DFT. We used a four-electron projected augmented pseudopotential for Si, with a plane-wave cutoff of 380 eV and Γ k-point sampling in the Brillouin zone (BZ). The FPMD simulations were performed in the canonical ensemble (constant N, V, and temperature, T) with Nose-Hoover thermostat and

*Contact author: bonev2@llnl.gov

 ©2024 American Physical Society

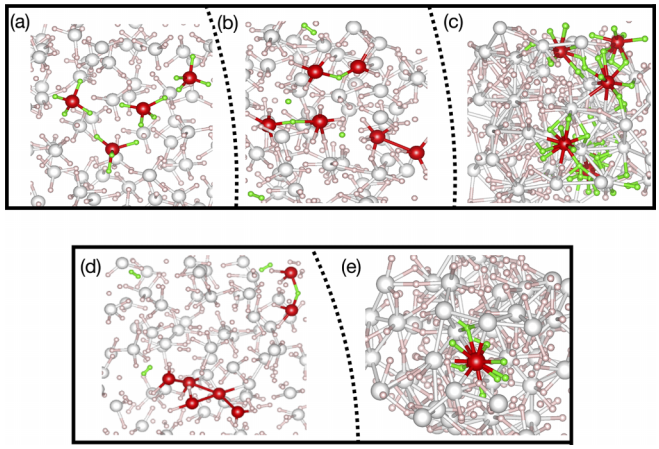

FIG. 1. Atomic configurations of liquid SiH_4 illustrating the structural transformations taking place as a function of pressure along the 1000 K isotherm at (a) 7.4 GPa, (b) 28 GPa, and (c) 178.5 GPa, and along 2000 K at (d) 8.3 GPa and (e) 193.7 GPa. Selected Si and H atoms are shown in red and green, respectively, illustrating the local order characteristic for each phase.

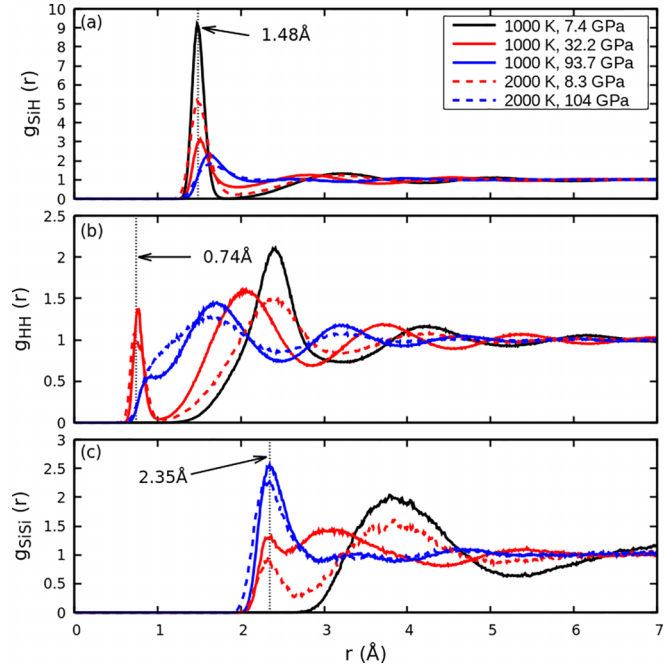

FIG. 2. Partial radial distribution functions of liquid SiH_4 at selected pressures at 1000 and 2000 K. The arrows and vertical dotted lines indicate equilibrium bond lengths of the SiH, H_2, and SiH_4 molecules at ambient conditions, which are 1.48 Å, 0.74 Å, and 2.35 Å, respectively. They are to be compared with the first peak of the radial distribution functions.

cubic supercells (with periodic boundary conditions) containing 64 SiH_4 units (320 atoms). At each density-temperature point considered, the simulations ran for 10 ps with an ionic time step 0.5 fs. The analysis was performed on the data collected after the initial 2 ps equilibration.

III. RESULTS

A. Structural properties

Under compression to 265 GPa ($r_s = 1.4$) at 1000 K, liquid SiH_4 exhibits three distinct phase regions with characteristic speciation and local order around the Si and H atoms. Figure 1 provides a visualization of these regions. At 1000 K, below 18 GPa the system remains molecular with intact, covalently bonded SiH_4 tetrahedra [Fig. 1(a)]. Above 18 GPa [Fig. 1(b)], we observe the formation of H_2 molecules, as well as longer Si polymers, connected either directly (Si-Si) or via bridging H atoms between them (Si-H-Si). Beyond 55 GPa [Fig. 1(c)], the free H_2 disappear, and instead there is a formation of longer polymers while the average coordination of the Si atoms gradually increases with pressure. Henceforth, we will refer to these three phases as molecular, mixed, and polymeric. Figures 1(d) and 1(e) depict the atomic configurations representing the mixed and polymeric phases at 2000 K. At the higher temperature, the phase transition to the mixed phase is shifted to significantly lower pressure compared to 1000 K; the H_2 molecules and Si-Si bonding are already observed at 8.3 GPa at 2000 K. However, the transition to the final polymeric phase does not exhibit any strong temperature dependency.

Partial (Si-H, H-H, and Si-Si) radial distribution functions are shown in Fig. 2. In the molecular and mixed phases, the nature of the Si-H bonding remains qualitatively unchanged [Fig. 2(a)], with bond distance comparable to the covalent bond in the SiH_4 tetrahedra at ambient conditions. Surprisingly, the decrease in the fraction of Si-H pairs during the molecular-to-mixed phase transition is accompanied by the formation of both H_2 and Si_2 pairs, as seen in Figs. 2(b) and 2(c). Notice that the location of the first peak of $g_{HH}(r)$ matches well the hydrogen molecular bond length and that of $g_{SiSi}(r)$ the Si-Si bond length at ambient conditions.

These characteristics of the mixed phase are present at both 1000 and 2000 K. Upon further compression to the polymeric phase above 55 GPa, the signature of H_2 disappears, while the continued growth of $g_{SiSi}(r)$ around 2.5 Å and the diminishing first peak of $g_{SiH}(r)$ suggest the formation of polymeric Si-Si chains and increased valency of Si. We note that the mixed phase, which is characterized by the presence of H_2 molecules, is different from the known high-pressure solid phases of SiH_4 below 250 GPa.

To quantify the types of bonding and species, which formed during the compression of liquid SiH_4, we have calculated the fractions of the relevant coordination configurations as a function of pressure (Fig. 3).

At pressure below 18 GPa at 1000 K [Fig. 3(a)], the SiH_4 fraction in the system is equal to unity, and the system is purely molecular. As the pressure increases along 1000 K and above 18 GPa, the SiH_4 break and there is an overall tendency of increasing Si-H coordination [Fig. 3(b)] as well as Si-Si bonding [Figs. 3(a) and 3(d)]. However, interestingly, this increase is not monotonic. Notice the dip in the $Si-H_5$, $Si-Si_x$, and $H-Si_x$ curves as a function of pressure, and the simultaneous peak in the $Si-H_2$ and $Si-H_3$ curves. In Fig. 3(c), we see that this is associated with the appearance of a significant amount of H_2 pairs, which peaks around 41 GPa at 1000 K. Thus, after the dissociation in the molecular liquid, as the pressure is increased, there is a narrow range where

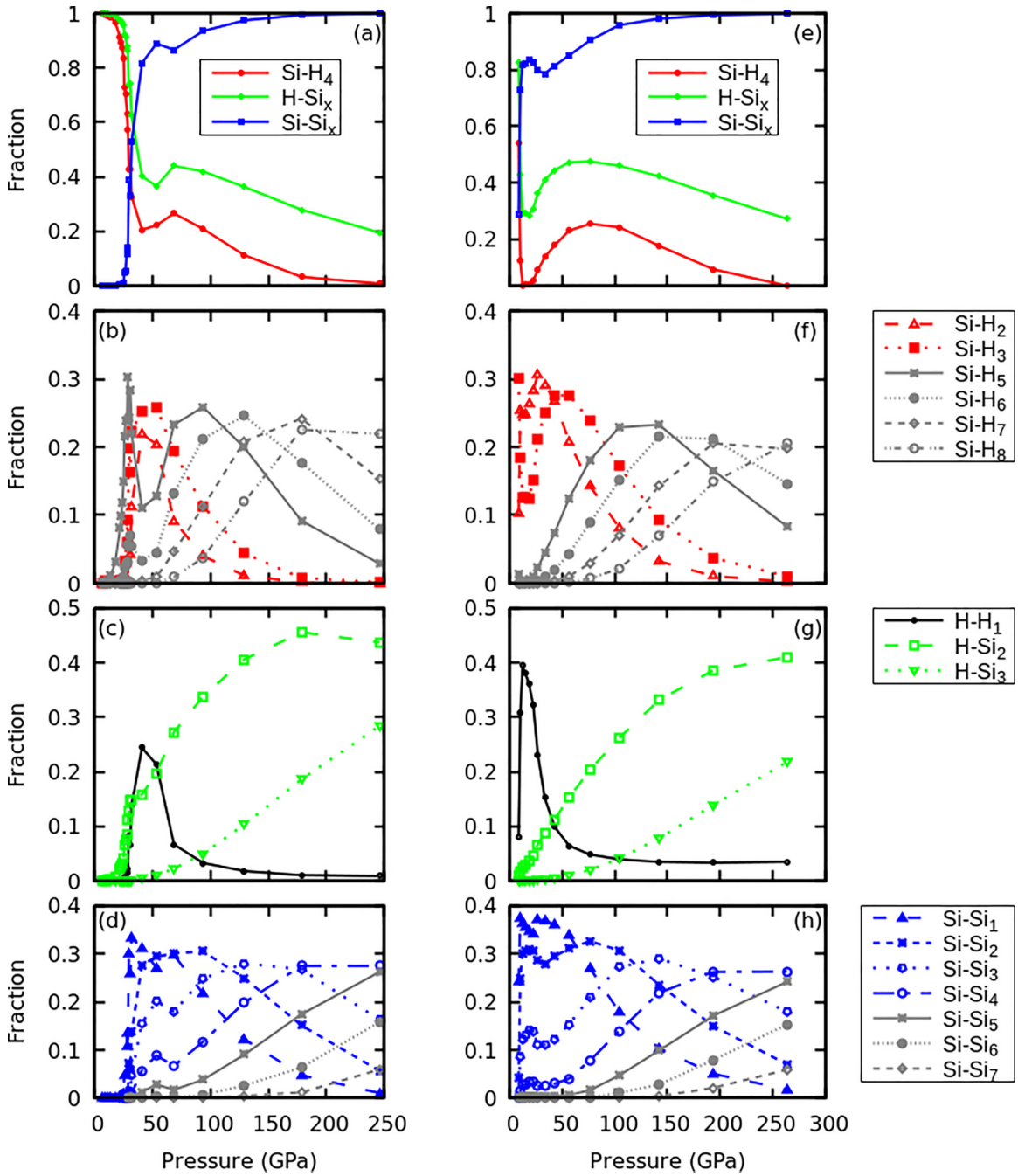

FIG. 3. Coordination fractions in liquid SiH_4 as a function of pressure along the 1000 (left column) and 2000 K (right column) isotherms. Here X-Y_n (where X, Y is either H or Si) indicates the average fraction of X atoms, which have n Y neighbors at the given P-T conditions and X-Y_x is the fraction of X atoms with Y neighbors regardless of their number. Coordination is computed by counting atoms within cutoff radii equal to 1.8, 0.8 and 2.45 Å for the Si-H, H-H and Si-Si pairs, respectively.

SiH_5 units with shared H atoms or connected with Si-Si bonds are the predominant species, which quickly gives way to a mixture of H_2 pairs and Si-H chains made of SiH_3 and SiH_2 units interconnected via Si-Si bonds or bridging H atoms (Si-H-Si). Above 53 GPa, as the amount of H_2 decreases, the Si-H coordination gradually increases and peaks sequentially into five-, six-, seven-, and eightfold coordinated Si with respect to H. The Si-Si coordination increases too, as longer polymers are being formed. At 2000 K (Fig. 3, right panel), the mixed phase emerges at significantly lower pressure. Notice also that the amount of H_2 is larger, while the initial surge in SiH_5 is not present. Instead, it is the fraction of SiH_3 which peaks initially and then dips as H_2 increases. Upon further compression, the transformations at 2000 K follow qualitatively that at 1000 K.

In solid silane, in comparison, SiH_4 tetrahedra were measured and also computed to persist up to 25 GPa [8,14]. This pressure is slightly higher compared to what we find in the liquid at 1000 K. Between 25–55 GPa, solid silane was reported [9] as a polymer made of SiH_6 units. In contrast, in the 1000 K

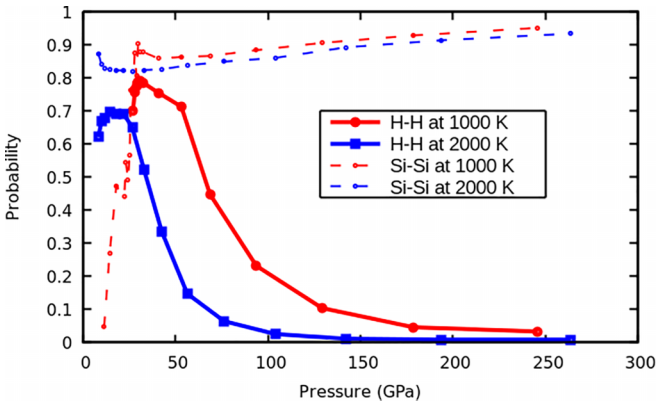

FIG. 4. Probability for H-H and Si-Si bonds to survive 20 fs (40 H_2 oscillations) after formation, as function of pressure. The calculation of this survival probability is explained in the text.

liquid we have the mixed phase in this pressure range, while the Si-H_6 coordination does not peak until about 150 GPa (though the overall coordination of Si, counting both H and Si, becomes sixfold at lower pressure). Above 53 GPa, crystalline silane was reported [8,9,16] a SiH_8 polymer. A polymeric solid phase with H_2 pairs within an Si-H network, similar to the liquid mixed phase, was predicted [15], but at much higher pressures, above 250 GPa. Additionally, the the Si atoms are 12-fold (hydrogen) coordinated in the mixed solid phase, while in liquid mixed phase there are predominantly SiH_3 and SiH4 units. Overall, there is a qualitative agreement between the solid and liquid phases for the increase of Si valency under compression, but the structural details vary and the pressures at which the mixed phases emerge are significantly different in the solid and the liquid.

B. Dynamical properties

The observed structural changes raise the question for the stability of the various bonds observed in the emerging nonmolecular phases. We evaluate the dynamical stability of a bond by its persistence or probability to survive a certain amount of time once it is formed. When the distance between a pair of atoms becomes smaller than a chosen cutoff distance, we consider that a bond has been formed. Here the focus is on the H-H and Si-Si pairs, for which we have chosen cutoff distances of 0.8 and 2.45 Å, respectively, or slightly larger than the equilibrium bond lengths of the H_2 and Si_2 molecules (see Fig. 2). The sensitivity of the results with respect to these values was tested to confirm that they do not change qualitatively when varying the cutoffs by a few percent. The time a bond survives is calculated as the time from which it is formed until the instance when the two atoms are found at a distance larger than the cutoff. We calculate the survival probability as the fraction of bonds which remain intact for time longer than 20 fs, which corresponds to 40 periods of H_2 oscillations in vacuum.

The survival probability of the H-H and Si-Si bonds as a function of pressure along the two isotherms are plotted in Fig. 4. The fact that the overall survival probabilities are higher at 1000 K than at 2000 K is not surprising; energy barriers are easier to overcome at higher T. What is interesting to note is the high stability of H-H bonds in the mixed phase. They have between 70 and 80% probability to survive 40 H_2 oscillations, confirming that the hydrogen pairs in this phase are not transient, but relatively stable molecules. The rapid rise in the stability of Si-Si precedes the appearance of H_2 molecules, after which it peaks and declines slightly with pressure in the mixed phase. Upon further compression, it increases monotonically into the region where there is a large formation of polymeric chains (above 50 GPa). Along 2000 K, we observe the same trends as at 1000 K, but the stability of the H_2 bond is shifted to lower pressure.

One way to detect and experimentally verify the predicted liquid phase transitions would be using vibrational spectroscopy. For this purpose, we have computed the vibrational density of states of the liquid. The results for the mixed and polymeric phases are shown in Fig. 5. The main characteristic of the mixed phase at both 1000 and 2000 K is the appearance of active modes in the region around 125 THz, which corresponds to the vibrational frequency of the H_2 molecule in gas [21]. Note that the vibrational frequency of H_2 in Si solid at ambient pressure has been measured [22] at 120 THz and calculated [23] at 104–134 THz (DFT is known to slightly underestimate the experimental values for the H_2 vibron). Furthermore, we see a slight shoulder in the Si-projected VDOS around 15 THz, corresponding to Si_2 modes, but these are unlikely to be detectable experimentally. The frequencies between around 60 to 70 THz are stretching modes of SiH_2, SiH_3, and SiH_5, and the region around 20 to 30 THz corresponds to their deformation modes. The transition to the polymeric phases is characterized by the disappearance of the peak at 60 THz and the H_2 modes above 100 THz.

C. Electronic properties

Since discovering and elucidating metallization is a main objective in studying hydrogen-rich systems, we have examined the electronic properties of SiH_4 as a function of pressure. The metallization of crystalline silane has been studied extensively, leading to somewhat conflicting results. Experimental works by Eremets *et al.* [10] and Chen *et al.* [8,10] reported it to metallize at 60 GPa, however, Degtyareva *et al.* [14] attributed the metallic silane phase at 60 GPa to platinum hydride. Theoretical work by Martinez-Canales *et al.* [9], predicted a metallic solid silane between 220–250 GPa. Later, Hanfland *et al.* [17] measured nonmetallic silane up to 130 GPa at room temperature.

The computed electronic density of states (EDOS) are shown in Fig. 6(a) at pressures near where the band gap closes, namely, 8.3 and 28 GPa at 1000 and 2000 K, respectively. Not surprisingly, the gap closure has a strong temperature dependence. For both temperatures, it takes place at significantly lower pressures in the liquid than what has been reported for solid SiH_4. The computed projected density of states at 1000 and 2000 K shown in Fig. 6(b) demonstrate that the gap closure is mainly due to overlapping p orbitals of the Si atoms.

Because GGA is well-known to underestimate band gaps, we have computed the EDOS with the hybrid exchange HSE06 functional using atomic configurations from the GGA

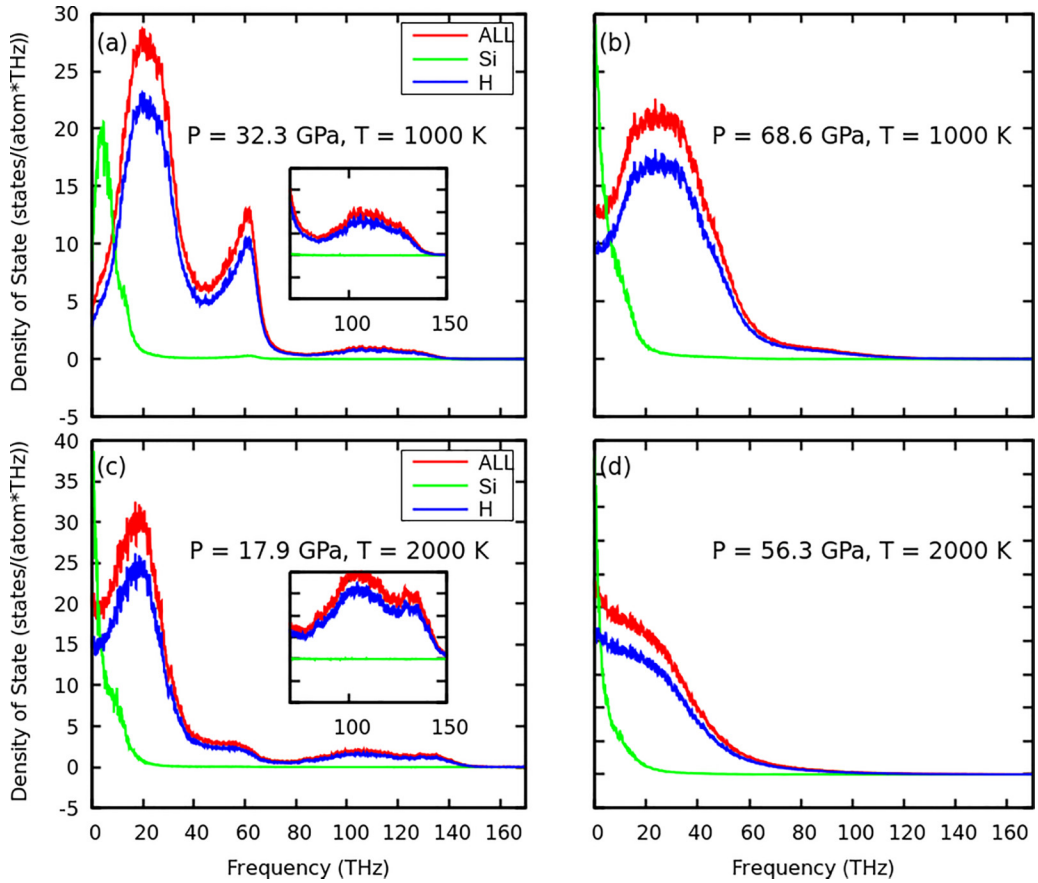

FIG. 5. Vibrational density of states (VDOS) at 1000 K in the (a) mixed and (b) polymeric phases, and at 2000 K in the (c) mixed and (d) polymeric phases. In addition to the total VDOS (red color), projected VDOS on the Si (green) and H (blue) atoms are shown as well. The insets show the region around 125 THz, which corresponds to the vibrational frequency of the H_2 molecule.

FPMD. The gap closure within HSE06 is delayed, but not significantly when compared to the metallization pressure in the solid phases. We note that if one is to perform FPMD within the HSE06 (or similar) functional, it is possible that the band closure would be further delayed to higher pressures. However, because the energy fluctuation $\langle (E_{\mathrm{GGA}} - E_{\mathrm{HSE}} - \langle E_{\mathrm{GGA}} - E_{\mathrm{HSE}} \rangle)^2 \rangle / 2k_B T$ is negligible, we do not expect the effect to be significant. Here E_{GGA} and E_{HSE} are energies of FPMD atomic configurations computed within GGA and HSE06, respectively, and $\langle\rangle$ is a statistical average over the GGA FPMD ensemble.

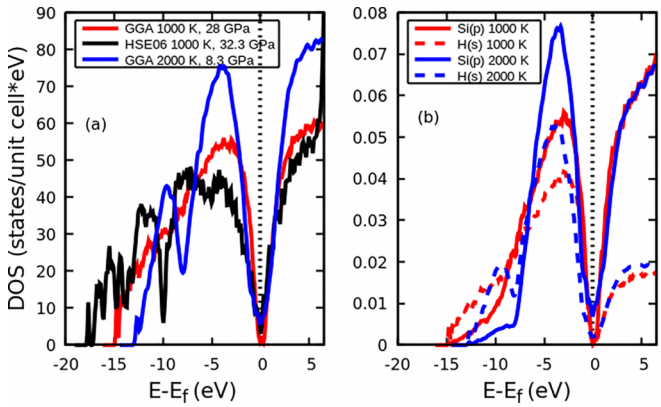

FIG. 6. Electronic density of states (EDOS): (a) total EDOS and (b) atom and angular-momentum (s, p) projected EDOS.

The electronic conductivity was evaluated at selected densities along the 1000 and 2000 K isotherms. Similarly to the EDOS, at each density considered, the conductivity was averaged over 10 to 12 well-spaced atomic configurations taken from the FPMD trajectories. For these calculations, a $2 \times 2 \times 2$ $\boldsymbol{k}$-point grid was used and the electronic orbitals were occupied based on a Fermi-Dirac distribution with an electronic temperature equal to the ionic temperature. The real part of the optical conductivity was obtained using the Kudo-Greenwood formula [24–27]:

$$\sigma_1(\omega) = \frac{2\pi e^2 \hbar^2}{3m^2 \omega \Omega} \sum_{\boldsymbol{k}} W(\boldsymbol{k}) \sum_{i,j=1}^{N} \sum_{\alpha=1}^{3} [F(\epsilon_i, \boldsymbol{k}) - F(\epsilon_j, \boldsymbol{k})] \times |\langle \psi_{j,\boldsymbol{k}} | \nabla_\alpha | \psi_{i,\boldsymbol{k}} \rangle|^2 \delta(\epsilon_{i,\boldsymbol{k}} - \epsilon_{j,\boldsymbol{k}} - \hbar\omega), \quad (1)$$

as implemented in VASP (the quantity calculated in VASP is the frequency-dependant dielectric function, $\epsilon(\omega) = \epsilon_1(\omega) + i\epsilon_2(\omega)$; $\sigma_1(\omega) = \epsilon_0 \omega \epsilon_2(\omega)$, where ϵ_0 is the vacuum permittivity). Here e and m are the electron charge and mass, Ω is the unit cell volume, the indices i and j label the electronic orbitals, α labels the spacial directions, and $F(\epsilon_i, \boldsymbol{k})$ is the occupation of the ith orbital at $\boldsymbol{k}$. $W(\boldsymbol{k})$ is the multiplicity

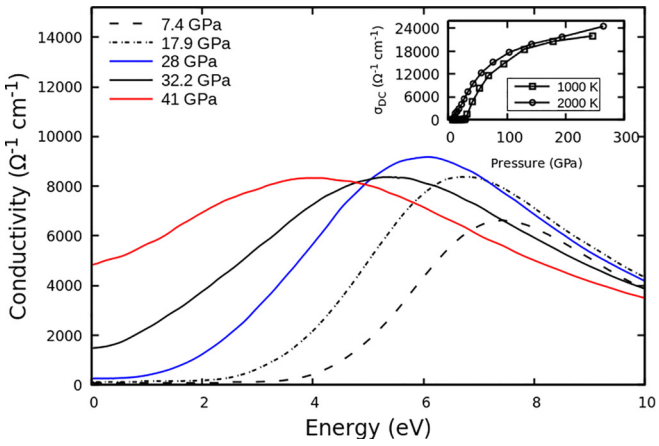

FIG. 7. Frequency-dependent conductivity of liquid silane at selected pressures at 1000 K. Inset: dc conductivity as a function of the pressure along the 1000 (squared) and 2000 K (circled) isotherms.

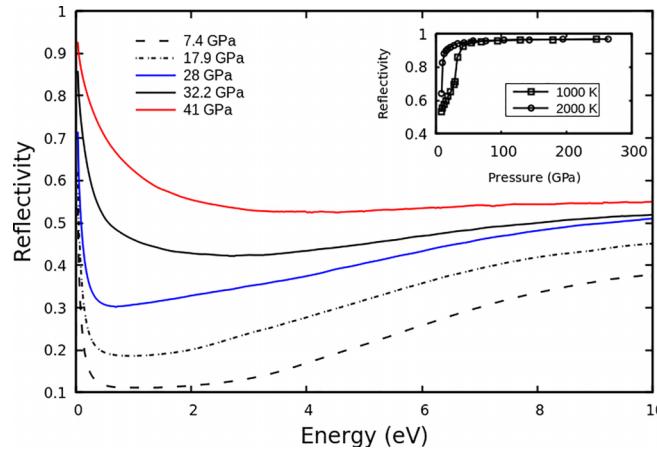

FIG. 8. Frequency-dependent reflectivity of liquid silane at selected pressures at 1000 K. Inset: Reflectivity as a function of the pressure along the 1000 (squared) and 2000 K (circled) isotherms.

(weight) of point $\boldsymbol{k}$ in the BZ. The zero-frequency limit of Eq. (1) yields the direct-current (dc) conductivity, $\sigma_{\rm dc}$.

The frequency-dependent conductivity of liquid silane for selected pressures at 1000 K is shown in Fig. 7. The peaks between 5 and 10 eV match well the EDOS profile around the Fermi level. The inset of Fig. 7 displays the dc conductivity along the 1000 and 2000 K isotherms. It becomes nonzero in the mixed phases with the onset of SiH_4 dissociation and band-gap closure, and increases with compression, eventually reaching 2×10^4 $\Omega^{-1}{\rm cm}^{-1}$ by 150 GPa. This value is comparable to the conductivity of metals, such as Ti at ambient conditions. For comparison, the conductivity of liquid metallic hydrogen in the temperature range between 1800 to 2700 K was recently measured [28] to be $11,000 \pm 1,100$ and $15,500 \pm 1,500$ $\Omega^{-1}{\rm cm}^{-1}$ at 140 and 170 GPa, respectively. It is also nearly an order of magnitude higher than the dc conductivity of liquid nitrogen [29,30] at similar conditions and liquid amorphous silicon [31] at 1800 K.

Our computed conductivity rises to significantly higher values with pressure than the reported experimental measurements [18]. In Ref. [18], the conductivity (resistivity) plateaus between 40 and 100 GPa, after which it further increases but does not reach the value reported here. In contrast, our calculations show that it increases continuously with pressure. This finding is consistent with our earlier observation about the band-gap closure originating from the overlap of Si p orbitals. The increasing Si-Si coordination and overlap of p orbitals under compression correlates well with the increasing dc conductivity. We emphasize that the metallization in liquid SiH_4 is not due to the hydrogen subsystem, as proposed in Ref. [18], but the formation of polymeric Si structures.

The experimental paper notes that silane keeps its molecular character up to 90 GPa, which could explain their resistivity findings in the pressure range from 40 to 100 GPa. However, this claim is an assumption based on the properties of crystalline silane and is not supported by our findings. A possible partial explanation for our differences with Ref. [18] may be the use of an approximate equation of state model in that work, which could lead to significant errors in the estimated experimental pressure and temperatures, especially for a dissociating fluid.

As the reflectivity is a common experimental observable, which is relatively easier to measure than the conductivity, we have computed it and are reporting it for comparison with future measurements. The frequency-dependent reflectivity, $R(w)$, can be obtained from the dielectric function as

$$\epsilon(\omega) = \epsilon_1(\omega) + i\epsilon_2(\omega) = [n(\omega) + ik(\omega)]^2, \tag{2}$$

$$R(\omega) = \frac{[1 - n(\omega)]^2 + k^2(\omega)}{[1 + n(\omega)]^2 + k^2(\omega)}. \tag{3}$$

It is plotted in Fig. 8 for several pressures at 1000 K. The reflectivity [zero-frequency limit of $R(\omega)$] is shown in the inset as a function of pressure along the 1000 and 2000 isotherms.

IV. CONCLUSION

We have reported FPMD simulations of liquid silane at temperatures of 1000 and 2000 K and pressures from (near) ambient to 265 GPa. The system is shown to transition from a molecular SiH_4 to a dense polymeric fluid with increasingly high Si coordination over this pressure range. A mixed phase consisting of H_2 molecules and shorter Si-H polymers is found at intermediate to low (at higher T) pressures. The H_2 pairs in this phase exhibit dynamical stability, being able to survive 40 vibron oscillations with 80% and 70% probability at 1000 and 2000 K, respectively. It would be interesting to evaluate in a follow-up work if this is indeed an equilibrium phase or its free energy of mixing is positive. For comparison, the mixed solid phase predicted above 250 GPa was determined to be equilibrium [15].

The electronic properties of liquid silane are analyzed as well, predicting that it metallizes in the mixed phase with the onset of polymerization due to overlapping Si p states. The dc conductivity of the fluid increases with compression, in parallel with the increasing Si-Si coordination. Our observations for the origin of conductivity in the fluid silane

differ from the interpretation of recent experimental measurements [18]. Our reported maximum dc conductivity is also larger than the experimental findings at similar conditions. We hope that this paper will stimulate further studies and the data provided here will help resolve the existing differences.

ACKNOWLEDGMENTS

This work was performed under the auspices of the US Department of Energy by Lawrence Livermore National Laboratory under Contract No. DE-AC52-07NA27344. The work was supported by NNSA Grant No. DE-NA0003984.

[1] N. W. Ashcroft, Phys. Rev. Lett. **92**, 187002 (2004).
[2] E. Wigner and H. Huntington, J. Chem. Phys. **3**, 764 (1935).
[3] N. W. Ashcroft, Phys. Rev. Lett. **21**, 1748 (1968).
[4] N. W. Ashcroft, J. Phys.: Condens. Matter **16**, S945 (2004).
[5] M. Martinez-Canales, A. Bergara, J. Feng, and W. Grochala, J. Phys. Chem. Solids **67**, 2095 (2006).
[6] G. Gao, A. R. Oganov, A. Bergara, M. Martinez-Canales, T. Cui, T. Iitaka, Y. Ma, and G. Zou, Phys. Rev. Lett. **101**, 107002 (2008).
[7] J. Feng, W. Grochala, T. Jaron, R. Hoffmann, A. Bergara, and N. W. Ashcroft, Phys. Rev. Lett. **96**, 017006 (2006).
[8] X. J. Chen, J. L. Wang, V. V. Struzhkin, H. K. Mao, R. J. Hemley, and H. Q. Lin, Phys. Rev. Lett. **101**, 077002 (2008).
[9] M. Martinez-Canales, A. R. Oganov, Y. Ma, Y. Yan, A. O. Lyakhov, and A. Bergara, Phys. Rev. Lett. **102**, 087005 (2009).
[10] M. I. Eremets, I. A. Trojan, S. A. Medvedev, J. S. Tse, and Y. Yao, Science **319**, 1506 (2008).
[11] Y. Yao, J. S. Tse, Y. Ma, and K. Tanaka, Europhys. Lett. **78**, 37003 (2007).
[12] X. J. Chen, V. V. Struzhkin, Y. Song, A. F. Goncharov, M. Ahart, Z. Liu, H. K. Mao, and R. J. Hemley, Proc. Natl. Acad. Sci. USA **105**, 20 (2008).
[13] C. Narayana, H. Luo, J. Orloff, and A. L. Ruoff, Nature (London) **393**, 46 (1998).
[14] O. Degtyareva, M. Martinez Canales, A. Bergara, X. J. Chen, Y. Song, V. V. Struzhkin, H. K. Mao, and R. J. Hemley, Phys. Rev. B **76**, 064123 (2007).
[15] W. Cui, J. Shi, H. Liu, Y. Yao, H. Wang, T. Itaka, and Y. Ma, Sci. Rep. **5**, 13039 (2015).
[16] C. J. Pickard and R. J. Needs, Phys. Rev. Lett. **97**, 045504 (2006).
[17] M. Hanfland, J. E. Proctor, C. L. Guillaume, O. Degtyareva, and E. Gregoryanz, Phys. Rev. Lett. **106**, 095503 (2011).
[18] Y.-G. Wang, F.-S. Liu, and Q.-J. Liu, Phys. B: Condens. Matter **541**, 89 (2018).
[19] G. Kresse and J. Furthmüller, Phys. Rev. B **54**, 11169 (1996).
[20] J. P. Perdew, K. Burke, and M. Ernzerhof, Phys. Rev. Lett. **77**, 3865 (1996).
[21] B. Stoicheff, Can. J. Phys. **35**, 730 (1957).
[22] K. Murakami, N. Fukata, S. Sasaki, K. Ishioka, M. Kitajima, S. Fujimura, J. Kikuchi, and H. Haneda, Phys. Rev. Lett. **77**, 3161 (1996).
[23] C. G. Van de Walle, Phys. Rev. Lett. **80**, 2177 (1998).
[24] D. Greenwood, Proc. Phys. Soc. **71**, 585 (1958).
[25] R. Kubo, J. Phys. Soc. Jpn. **12**, 570 (1957).
[26] D. A. Horner, J. D. Kress, and L. A. Collins, Phys. Rev. B **77**, 064102 (2008).
[27] B. Holst, R. Redmer, and M. P. Desjarlais, Phys. Rev. B **77**, 184201 (2008).
[28] M. Zaghoo and I. F. Silvera, Proc. Natl. Acad. Sci. USA **114**, 11873 (2017).
[29] W. J. Nellis, S. T. Weir, and A. C. Mitchell, Phys. Rev. B **59**, 3434 (1999).
[30] B. Boates and S. A. Bonev, Phys. Rev. B **83**, 174114 (2011).
[31] T. A. Abtew, M. Zhang, and D. A. Drabold, Phys. Rev. B **76**, 045212 (2007).